JMEPEG (2011) 20:865–876
DOI: 10.1007/s11665-010-9727-9

1059-9495/$19.00

Finite Element Simulations for Investigating the Effects of Specimen Geometry in Superplastic Tensile Tests

Mohammad Nazzal, Fadi Abu-Farha, and Richard Curtis

(Submitted December 5, 2009; in revised form June 8, 2010)

Characterizing the behavior of superplastic materials is largely based on the uniaxial tensile test; yet the unique nature of these materials requires a particularly tailored testing methodology, different to that used with conventional materials. One of the crucial testing facets is the specimen geometry, which has a great impact on the outcome of a superplastic tensile test, as a result of the associated extreme conditions. And while researchers agree that it should take a notably different form than the typical dog-bone shape; there is no universal agreement on the specimen's particular size and dimensions, as evident by the disparities in test specimens used in the various superplastic testing efforts found throughout the literature. In view of that, this article is dedicated to understanding the effects of specimen geometry on the superplastic behavior of the material during tensile testing. Deformation of the Ti6Al4V titanium alloy is FE simulated based on a multitude of specimen geometries, covering a wide range of gauge length, gauge width, grip length, and grip width values. The study provides key insights on the influences of each geometrical parameter as well as their interactions, and provides recommendations on selecting the specimen's proportions for accurate and unified tensile testing of superplastic materials.

Keywords elevated temperature tensile testing, finite element simulations, material flow, specimen geometry, superplastic materials

1. Introduction

Uniaxial tensile testing is still the dominant means for characterizing the behavior of superplastic materials; the unique class of materials that exhibits extraordinarily large and uniform ductility at relatively high temperatures and controlled deformation rates. This is particularly true for developing accurate constitutive models, which are the backbones of the finite element models we rely on for simulating, controlling, and optimizing superplastic forming processes. Naturally, the accuracy of those models depends on the accuracy of the tensile tests; and while tensile testing of typical engineering materials is a long-established and universally agreed on procedure, that is not the case with superplastic materials. Disparities in testing procedures and methodologies are clearly observed among the various efforts in the literature, often leading to differences in the collected data, even when investigating the same material. On top of the heating and holding time issues, adopting a variety of test specimen geometries is one of the clearest and most detrimental forms of discrepancy.

Mohammad Nazzal, School of Technological Sciences, German-Jordanian University, Amman, Jordan; **Fadi Abu-Farha**, Department of Mechanical Engineering, Penn State Erie, 5101 Jordan Road, 246 REDC Building, Erie, PA 16563; and **Richard Curtis**, King's College Dental Institute, King's College London, London, UK. Contact e-mails: mohammad.nazzal@gju.edu.jo, fka10@psu.edu, and Richard.curtis@kcl.ac.uk.

Since no superplastic testing standards were available before the year 2002, it is possible to attribute the disagreements on such crucial testing issues to the lack of standards. Ever since, though, three major standards on the proper method for testing superplastic materials in tension were introduced: the JIS H 7501, the ASTM E2448, and the BS ISO 20032 (Ref 1-3). Unhappily, the standards do not agree on several testing aspects; the most controversial ones in particular. In addition, they do not offer any reasoning to how the suggested testing parameters were selected, especially the dimensions and proportions of the test specimen. Whether it is due to their recent publication, the lack of comprehensiveness, or their apparent disagreements; the arrival of standards has not had a great impact, and most efforts on characterizing the behaviors of superplastic materials are still scattered. Selected examples of recent efforts in the field show that the investigators utilized test specimens with different gauge lengths; varying from a nominal 25 mm, to gauge lengths as small as 5 mm (Ref 4-8).

It is probably tolerable to presume that the size of a tensile test specimen is not greatly influential to the obtained stresses and strains. Measured forces and displacements, from which the latter are derived, are correlated to the initial size of the specimen's gauge section anyway. Nevertheless, the story is quite different when testing superplastic materials, simply because of the relatively high temperatures and the substantially large strains. The visco-plastic nature of superplastic materials causes unavoidable material flow from the grip region into the gauge region of the test specimen. This could be a major source of errors in the captured stress/strain behavior (Ref 9), hence indicating the need to optimize the proportions of the specimen geometry. It is such issues, unique to superplastic materials, which motivated the design of grips particularly tailored for superplastic tensile testing (Ref 10).

While the vast majority of superplastic testing efforts have been directed toward characterizing the behaviors of these

materials, only a handful targeted understanding the effects of specimen geometry on the test results. Johnson et al. (Ref 9) conducted both FE simulations and experiments on few AA 5083 tensile specimens, with various gauge length-to-width ratios, to investigate the end effects on strain rate within the gauge length of each specimen. The work concluded with an improved geometry that provides a constant strain rate in a major portion of the specimen's gauge. Bate et al. (Ref 11), on the other hand, explored the geometry's impact on deformation homogeneity and stress/strain curves, considering three AA 5083 specimens with different gauge length-to-width ratios. They proposed a correction to the stress stress/strain curves as a means to overcome the geometry's effects, particularly the associated material flow issue. It is efforts as such that we build on in the current work, in search of a broader understanding of geometry effects on the uniaxial tensile testing of superplastic materials.

As the aforementioned efforts consider a handful of specimen geometries, this article presents a rather comprehensive investigation, in which more than 30 specimen geometries are considered. Major attention is directed to the two key geometrical parameters, the gauge length and gauge width, by covering wide-ranging combinations of the two. And since the size of the grip region has not been previously investigated, multiple specimens are allotted for combinations of grip length and width values. Finite element analyses are carried out to simulate stretching of the specimens, using an advanced constitutive model for the Ti6Al4V titanium alloy; a material selected for its excellent superplastic behavior. In each simulation, the strain distribution along the gauge length of the deformed specimen, as well as material flow from the grip region into the gauge region, are quantified. Ultimately, the results are correlated to the geometrical parameters and their ratios, hence providing guidelines for selecting the optimum proportions of a "proper" specimen for accurate tensile testing of superplastic materials.

2. Test Specimen Geometries

The specimens covered in this investigation share the overall geometry shown in Fig. 1. It is based on a previous effort by the investigators, and resembles the geometries found in the major superplastic testing standards (Ref 1-3). In addition, it is compatible with a recently developed set of quick-mount grips, designed specifically to overcome major issues encountered in superplastic tensile testing (Ref 10). While the thickness and fillet radii are fixed, the remaining four geometrical parameters are variable, and they are:

l: gauge length
w: gauge width
l': grip length
w': grip width

Furthermore, it is believed that the interactions between these parameters are equally important, and thus three aspect ratios are defined as:

AR-Gauge (gauge region's aspect ratio) = l/w
AR-Grip (grip region's aspect ratio) = l'/w'
AR-GG (grip-to-gauge region aspect ratio) = w'/w

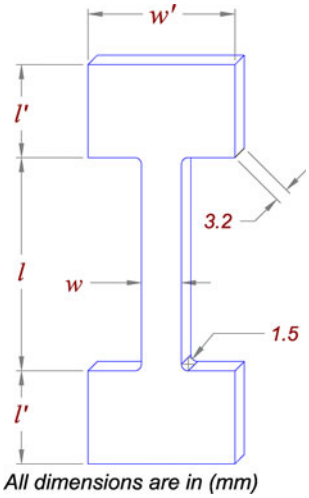

Fig. 1 Overall test specimen geometry highlighting the main parameters

Table 1 List of the various numerical values assigned for the four geometrical parameters

	Assigned values, mm			
No.	***l***	***w***	***l′***	***w′***
1	6	3	12	18
2	12	6	16	24
3	18	9	20	30
4	24	12	24	
5	30			
6	36			

These ratios will provide the basis for selecting the appropriate proportions of the desired tensile specimen geometry.

Table 1 summarizes the various numerical values assigned to each of the four geometrical parameters. As noted, wide-ranging values are considered, especially for the gauge area's parameters. These values are not randomly chosen; they are centered around the nominal specimen geometries of the major testing standards. The variations are selected at fixed intervals such that the majority of the geometries found in the literature are covered.

With a large number of possible combinations, it was necessary to focus on investigating the effects of a specific geometrical parameter or a ratio, one at a time. Therefore, the specimens were clustered in groups; each is characterized by the variability of a particular parameter. The selected groups are listed in Table 2, showing the values of the four parameters and the corresponding aspect ratios for each case. Each specimen is designated by $(l_i w_j - l'_m w'_n)$, where each of (i, j, m, n) denotes the number in Table 1 that corresponds to a parameter's specific numerical value.

3. Finite Element Model

The Finite element (FE) simulations were performed using the commercial code ABAQUS version 6.8. Figure 2 shows the

Table 2 List of designations and the corresponding geometrical parameters for the specimens covered in this investigation

Sets	Specimen designation	l, mm	w, mm	l', mm	w', mm	AR-Gauge	AR-Grip	AR-GG
Fix grip w_1 = 3 mm vary l	$l_1w_1 - l'_2w'_2$	6	3	16	24	2	0.67	8
	$l_2w_1 - l'_2w'_2$	12	3	16	24	4	0.67	8
	$l_3w_1 - l'_2w'_2$	18	3	16	24	6	0.67	8
	$l_4w_1 - l'_2w'_2$	24	3	16	24	8	0.67	8
	$l_5w_1 - l'_2w'_2$	30	3	16	24	10	0.67	8
	$l_6w_1 - l'_2w'_2$	36	3	16	24	12	0.67	8
Fix grip w_2 = 6 mm vary l	$l_1w_2 - l'_2w'_2$	6	6	16	24	1	0.67	4
	$l_2w_2 - l'_2w'_2$	12	6	16	24	2	0.67	4
	$l_3w_2 - l'_2w'_2$	18	6	16	24	3	0.67	4
	$l_4w_2 - l'_2w'_2$	24	6	16	24	4	0.67	4
	$l_5w_2 - l'_2w'_2$	30	6	16	24	5	0.67	4
	$l_6w_2 - l'_2w'_2$	36	6	16	24	6	0.67	4
Fix grip w_3 = 9 mm vary l	$l_1w_3 - l'_2w'_2$	6	9	16	24	0.667	0.67	2.667
	$l_2w_3 - l'_2w'_2$	12	9	16	24	1.333	0.67	2.667
	$l_3w_3 - l'_2w'_2$	18	9	16	24	2	0.67	2.667
	$l_4w_3 - l'_2w'_2$	24	9	16	24	2.667	0.67	2.667
	$l_5w_3 - l'_2w'_2$	30	9	16	24	3.333	0.67	2.667
	$l_6w_3 - l'_2w'_2$	36	9	16	24	4	0.67	2.667
Fix gauge w_4 = 12 mm vary l	$l_1w_4 - l'_2w'_2$	6	12	16	24	0.5	0.67	2
	$l_2w_4 - l'_2w'_2$	12	12	16	24	1	0.67	2
	$l_3w_4 - l'_2w'_2$	18	12	16	24	1.5	0.67	2
	$l_4w_4 - l'_2w'_2$	24	12	16	24	2	0.67	2
	$l_5w_4 - l'_2w'_2$	30	12	16	24	2.5	0.67	2
	$l_6w_4 - l'_2w'_2$	36	12	16	24	3	0.67	2
Fix gauge w'_1 = 18 mm vary l'	$l_5w_2 - l'_1w'_1$	30	6	12	18	5	0.67	3
	$l_5w_2 - l'_2w'_1$	30	6	16	18	5	0.89	3
	$l_5w_2 - l'_3w'_1$	30	6	20	18	5	1.11	3
	$l_5w_2 - l'_4w'_1$	30	6	24	18	5	1.33	3
Fix gauge w'_2 = 24 mm vary l'	$l_5w_2 - l'_1w'_2$	30	6	12	24	5	0.50	4
	$l_5w_2 - l'_2w'_2$	30	6	16	24	5	0.67	4
	$l_5w_2 - l'_3w'_2$	30	6	20	24	5	0.83	4
	$l_5w_2 - l'_4w'_2$	30	6	24	24	5	1.00	4
Fix gauge w'_3 = 30 mm vary l'	$l_5w_2 - l'_1w'_3$	30	6	12	30	5	0.40	5
	$l_5w_2 - l'_2w'_3$	30	6	16	30	5	0.53	5
	$l_5w_2 - l'_3w'_3$	30	6	20	30	5	0.67	5
	$l_5w_2 - l'_4w'_3$	30	6	24	30	5	0.80	5

FE geometrical model, which consists mainly of the test specimen and the grip. As noted, the selected model is three-dimensional, and accounts even for the depth dimension (thickness) of the specimen; this is to provide a better picture of material deformation. The specimen is modelled using 8-node brick elements, employing a fine (~0.5 to 1 mm per element) mesh. Symmetry is applied along three orthogonal planes to reduce simulation time; hence, only one-eighth of the specimen is actually shown in Fig. 2. The grip, on the other hand, is modelled as a rigid body; it is moved at a controlled rate during each simulation to initiate deformation in the specimen, hence simulating an actual tensile test. Only the shoulder of the grip is considered, since it is the part actually interacting with the specimen during deformation. A friction coefficient $\mu = 0.4$ is applied at the interface; this high value is based on a recent investigation by the authors that indicates near-sticking conditions to take place at the shoulder of the specimen, regardless of the surface conditions of both the specimen and the grip.

In each prospective simulation, the targeted outcomes were identified as: (1) evaluation of deformation and its uniformity in the gauge region, (2) evaluation of material flow from the grip region into the gauge region, and its impact on the obtained strains. To facilitate that, a virtual partition is applied to each specimen between the gauge and the grip regions, as shown in Fig. 2. By doing so, it is possible to focus on the deformation of the elements within the gauge region, hence establish the desired strain distribution. On the other hand, the distortion of the grip region's elements and their displacements can be tracked to establish the sought amount of material flow.

The Ti6Al4V alloy, one of the most commonly formed superplastic materials, was selected for this investigation, due to its excellent superplastic properties and extreme ductility limits. The following microstructure-based constitutive model was fed into the FE code through user-defined subroutines, to capture the behavior of the material at 900 °C (Ref 12):

$$\dot{\varepsilon} = \frac{C_i}{d^p}[\sigma - \sigma_0]^{1/m} + C_{ii}\sigma^n \qquad \text{(Eq 1)}$$

where $\dot{\varepsilon}$ is the effective strain rate, σ is the flow stress, σ_0 is the threshold stress, d is the grain size, m is the strain rate sensitivity index, and n is the strain hardening exponent. C_i, C_{ii}, and p are material constants.

4. Simulation Results and Discussion

All the simulations were carried out at a fixed speed corresponding to an initial strain rate of 5×10^{-4} s^{-1}. The reason for simulating at a fixed speed, instead of a fixed strain rate—the common way of conducting a superplastic tensile test is to try and make the study less dependent on a particular strain rate. A constant speed test is a variable strain rate test; and so by picking the speed such that it corresponds to an initially moderate strain rate, the strain rate at the end of the simulation would be smaller. By doing so, the simulation can be selectively controlled to cover an entire range of strain rates over which the material exhibits excellent superplastic behavior. In this study, the simulations will effectively cover strain rates ranging between 5×10^{-4} and 7.5×10^{-5} s^{-1}.

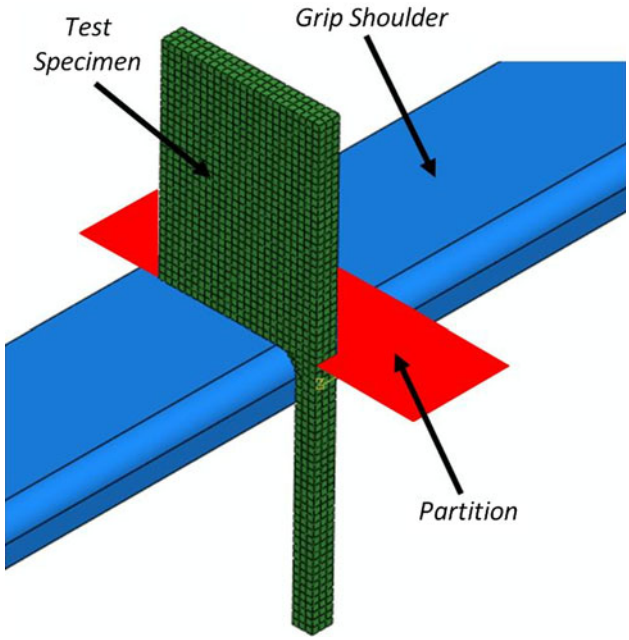

Fig. 2 3D finite element geometrical model with a partition imposed between the grip and the gauge regions

4.1 Selecting a Simulation Strategy

Since the performance of different specimen geometries are to be evaluated, it is important to specify the end condition for the simulations, to ensure fair basis of comparison. In pursuing that, two scenarios were considered, where the specimens are stretched at a fixed rate until:

I. The maximum localized strain, anywhere in the specimen's gauge, reaches a pre-set value (*limit*).
II. The overall theoretical strain in the specimen reaches a pre-set value.

The difference between the two is critical, and it is based on the way the deformation process is pictured. In the first scenario (I), the FE code is instructed to stretch the specimen while monitoring the strain in each element within the gauge region; as soon as any element undergoes a pre-defined maximum strain level, the simulation is stopped. This approach is practically inaccurate, because it is not feasible to conduct a tensile test in this manner, unless a laser extensometer or an in situ optical strain measurement system is used. The second scenario (II), on the other hand, is a reflection of how a tensile test is typically conducted; the operator has no control over the strain distribution along the gauge length, and all he does is to maintain deformation until a certain pre-defined theoretical strain value is reached. The latter is simply defined, based on the initial geometry of the specimen, as:

$$\varepsilon_{\text{Theor}} = \ln\left(\frac{l_f}{l}\right) \qquad \text{(Eq 2)}$$

where l and l_f are the initial and final gauge length values, respectively.

Although the second scenario is what we are practically looking for, we shall devote a portion of this investigation to highlighting the differences in results between the two approaches. Though the first approach is not practical, it still has some merits over the second one, from a material-failure perspective. Targeting an overall theoretical strain in different geometries will not yield the same maximum localized strain, and the latter is what defines when the material fails.

In this part, the focus is directed to a selected set of specimens, having identical geometries except for the gauge length, which progressively changes from 6 to 36 mm. The set is shown in Fig. 3, and corresponds to the second group of

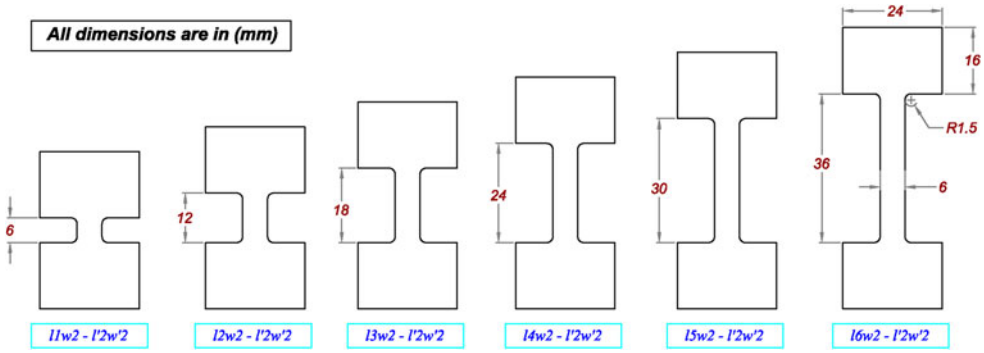

Fig. 3 Six identical specimens except for the gauge length changing between 6 and 36 mm (the gauge width is 6 mm)

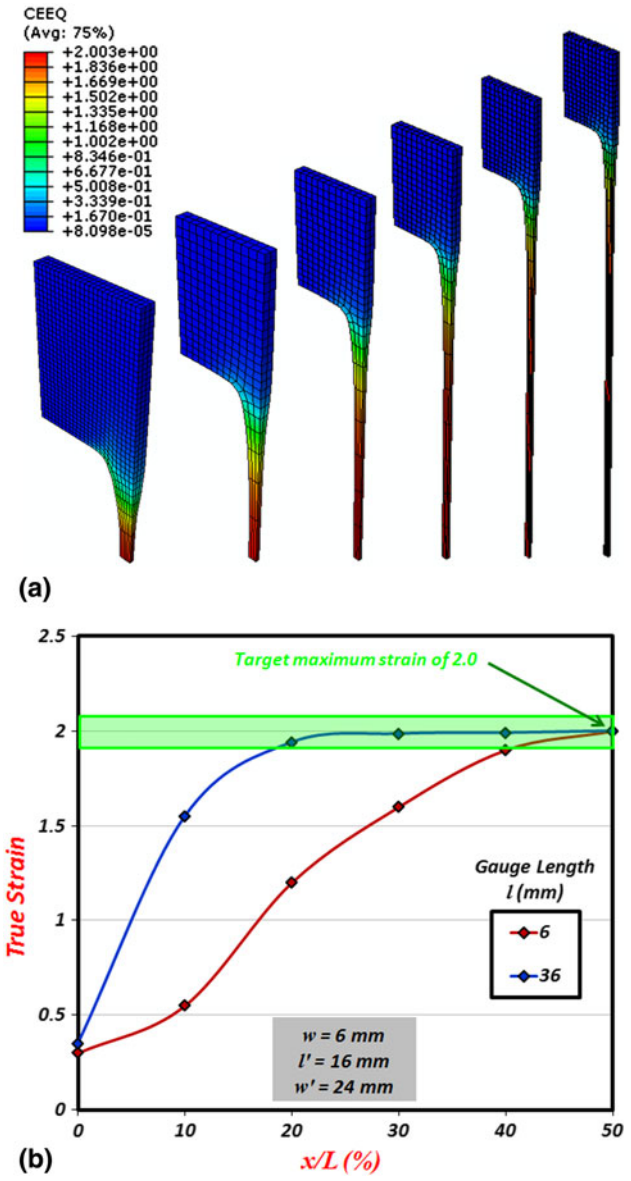

Fig. 4 (a) The six specimens in Fig. 3 after stretching to a maximum true strain of 2.0 (b) the corresponding final strain distribution in the short and long specimens

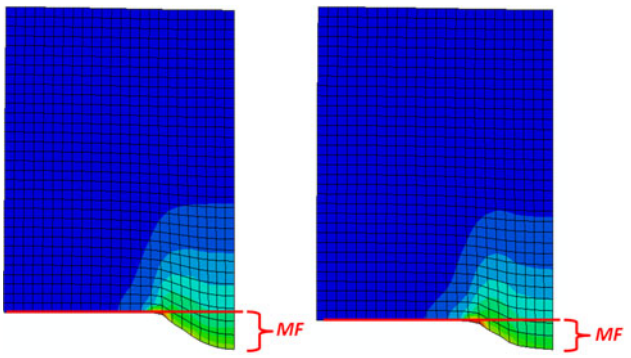

Fig. 5 Material flow from the grip region into the gauge region for the 6 mm (left) and 36 mm long specimen (right), after stretching to a maximum strain of 2.0

specimens in Table 2. In the first approach, the specimens were stretched at a fixed rate corresponding to an initial strain rate of 5×10^{-4} s^{-1} until a maximum strain value of 2.0 (≈640% elongation) is reached anywhere along the specimen's gauge. The resulting deformed specimens are shown in Fig. 4(a). The first obvious means of comparison is the uniformity of strain along the gauge length, which is straightforwardly based on the strain contour maps like the ones shown in the figure. Obviously, all the specimens reached a 2.0 strain right at the

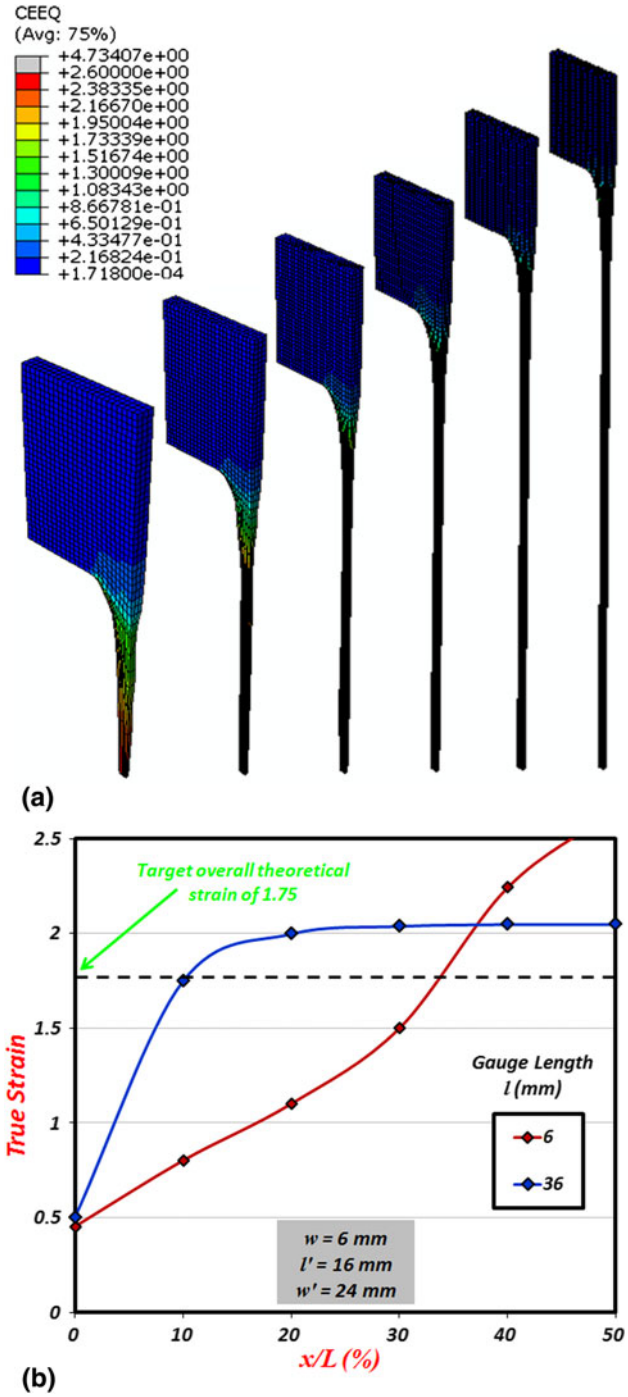

Fig. 6 (a) The six specimens in Fig. 3 after stretching to an overall theoretical strain of 1.75 (b) the corresponding final strain distribution in the short and long specimens

middle of the gauge length, since this is where maximum deformation is expected to take place. The remaining part of the gauge length will experience lower strain levels, in a decreasing manner as we approach the shoulder. By plotting the strain distribution along the entire gauge length, we can identify the percentage of the gauge length along which uniform strains are observed. Figure 4(b), for instance, provides a comparison between the shortest (6 mm) and longest (36 mm) specimens. Note that strain is considered to be uniform so long it falls within 5% of the targeted value (shown as the shaded area around a strain of 2.0).

It is observed that the long specimen exhibits uniform strains over approximately 70% of the gauge length, compared to no more than 20% in the case of the short specimen. A look back at Fig. 4(a) qualitatively supports the result. This suggests that a higher initial gauge length yields uniform strains over a larger portion of the specimen's gauge. Yet to be more precise, the previous statement should be translated in terms of the gauge length-to-width ratio, defined earlier as AR-Gauge. That is, the higher the AR-gauge ratio, the more uniform the deformation is expected to be within the specimen's gauge. For the considered specimens, this ratio varied between 1 for the short, and 6 for the long specimen.

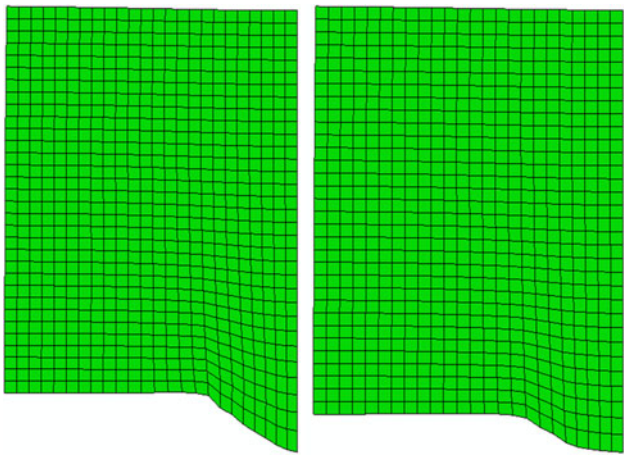

Fig. 7 Material flow from the grip region into the gauge region for the 6 mm (left) and 36 mm long specimen (right), after stretching to an overall theoretical strain of 1.75

As for material flow from the grip region into the gauge region, it can be observed, though not clear, in the deformed specimens in Fig. 4(a). With the aforementioned partition between the two regions, a closer look at deformation and distortion of the grip region can be realized. An example is shown in Fig. 5, which focuses on the grip area for both the short (6 mm) and the long (36 mm) specimens, after being strained to the same maximum localized strain of 2.0. It can be seen here that the material drew further into the gauge area in the case of the short specimen, in comparison with that in the long one. This material flow (denoted MF in the figure) was quantified as 3.8 mm for the short, and 2.9 mm for the long specimen. The difference is small, yet more important than the absolute value is the corresponding influence on the strains measured in the gauge section of each specimen. 3.8 mm flow in the short specimen represents 63.3% of its initial gauge length, while 2.9 mm flow in the long specimen represents only 8%. When subtracting this material flow from the specimen's final length, the corrected theoretical strain can be calculated as follows:

$$\text{Corrected } \varepsilon_{\text{Theor}} = \ln\left(\frac{l_f - \text{MF}}{l}\right) \qquad \text{(Eq 3)}$$

Accordingly, the error in the theoretical strain associated with material flow is estimated by comparing the strains of Eq 2 and 3; the 3.8 mm flow in the short specimen represents ≈23.5% error, while the 2.9 mm in the case of the long specimen represents an error of less than 1%.

While this approach of quantifying the amount of material flow (MF) into the gauge region, and then estimating the corresponding error in the measured strains, is just an approximation; it seems to provide a powerful tool for comparing between the multiple geometries, hence will be used in the all the prospective simulations.

The previous simulation approach does not lead to equivalent overall theoretical strains in the specimens with different gauge lengths; the short specimen reached an overall strain of 1.16, compared to 1.70 in the long specimen. This makes the simulation highly dependent on the degree of strain localization

Table 3 Summary of the FE simulation results for the two selected specimens (the 6 and 36 mm long specimens of Fig. 3) following two simulation strategies: one targeting a maximum localized strain, and another targeting an overall theoretical strain

	FE simulations targeting a maximum localized strain		FE simulations targeting an overall theoretical strain	
Specimen geometry:	$l_1w_2 - l'_2w'_2$	$l_6w_2 - l'_2w'_2$	$l_1w_2 - l'_2w'_2$	$l_6w_2 - l'_2w'_2$
Initial gauge length l_0, mm	6	36	6	36
Final length l_f, mm	19.2	196	34.53	207.17
Overall theoretical strain	1.163	1.695	1.75	1.75
Maximum localized strain	2.0	2.0	2.58	2.05
Strain deviation, %	72.0	18.0	47.4	17.1
Portion of gauge length with uniform strains, %	≈20	≈70	<10	≈70
Material flow (MF), mm	3.8	2.9	5.1	3
MF to l_0 ratio, %	63.33	8.06	85.0	8.33
Corrected l_f, mm	15.4	193.1	29.43	204.17
Overall theoretical strain after subtracting MF	0.942	1.68	1.59	1.735
Estimated error in overall theoretical strain, %	23.5	0.9	10.1	0.9

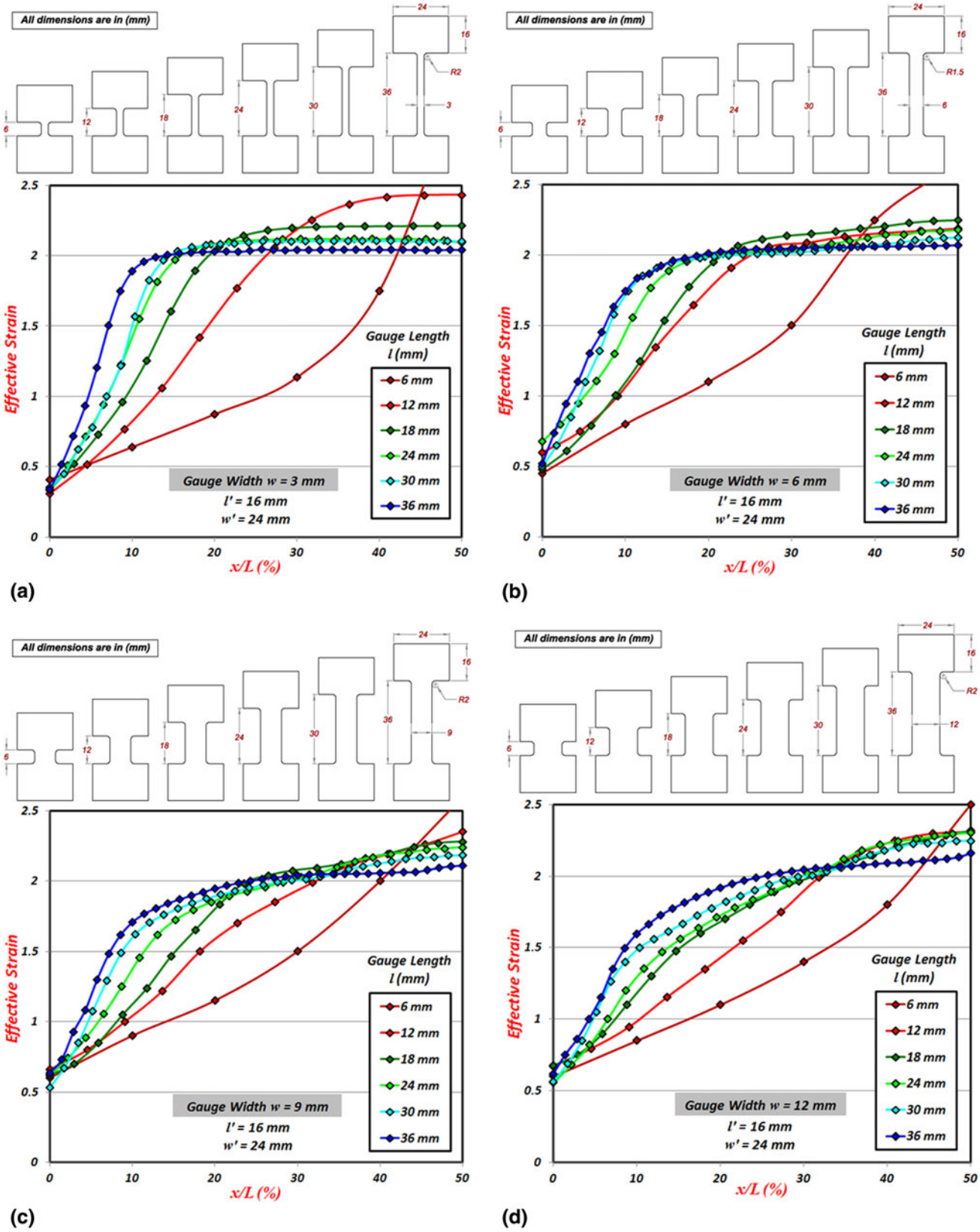

Fig. 8 Final strain distributions in specimens with various gauge lengths, for a gauge width of (a) 3 mm (b) 6 mm (c) 9 mm (d) 12 mm

in the specimen. So, the second approach is applied next, where the same six specimens in Fig. 3 are stretched until an overall theoretical strain value is reached. Since the gauge length is expected to exhibit varying strain levels (lower than the theoretical value closer to the shoulder, and higher than the theoretical value toward the middle of the gauge length),

a target strain value of 1.75 (close to 500% elongation) was chosen. Figure 6(a) shows the six deformed specimens, where the color coding shows that strains in excess of 2.5 were reached in some specimens. By focusing on the shortest and longest specimens, the difference between the two geometries is more prominent, since the short specimen developed a maximum localized strain of 2.58, compared to 1.92 in the long one. Doing so, one may quantify the error in achieving the targeted strain of 1.75 as 47% in the case of the short specimen, versus 9.7% in the case of the long specimen.

To further emphasize the aforementioned, a clearer picture is obtained by plotting the strain distribution along the specimen gauge, as shown in Fig. 6(b). This plot clearly demonstrates the percentage of the gauge length along which uniform strains are observed. Notice how the long specimen exhibits a uniform strain over ~70% of the gauge length, while the short one hardly shows any deformation uniformity.

As for material flow, Fig. 7 shows a similar comparison to the one presented earlier in Fig. 5. The material drew further into the gauge area in the case of the short specimen (≈5.1 mm), in comparison with that in the long one (≈3.0 mm). These figures mean that the flow in the short specimen represents about 85% of its initial gauge length, compared to 8.3% for the long one. Moreover, by calculating the corrected strains according to Eq 3, the 5.1 mm flow in the short specimen represents ≈10% error, while the error in the case of the long specimen remains below 1%.

Finally, a summary of the differences in the results following the two strategies is provided in Table 3. Note that the short specimen shows a greater difference between the maximum localized strain and the overall theoretical strain. In the first approach, in particular, that specimen achieved an overall strain of 1.163 for a maximum localized strain of 2.0, which represents about 72% deviation. And although the same specimen undergoes higher deformation in the second approach, reaching a maximum strain of 2.58, the deviation is actually smaller at about 47%. The long specimen, on the other hand, maintains about 18% deviation in both cases. The

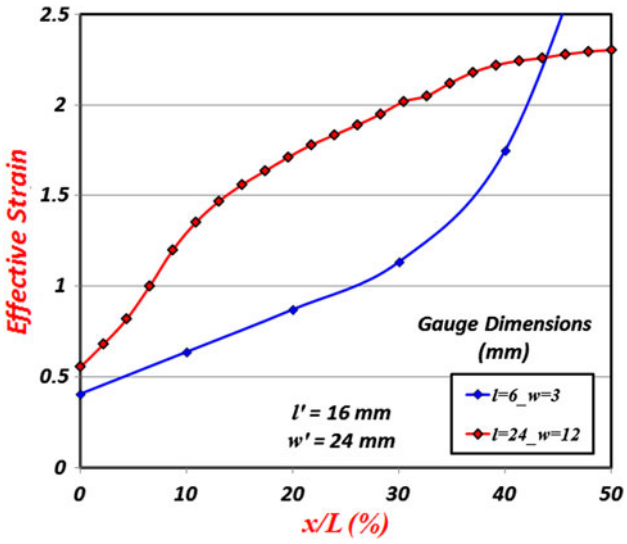

Fig. 9 Comparison of final strain distribution in two specimens with different gauge proportions yet the same AR-gauge ratio of 2

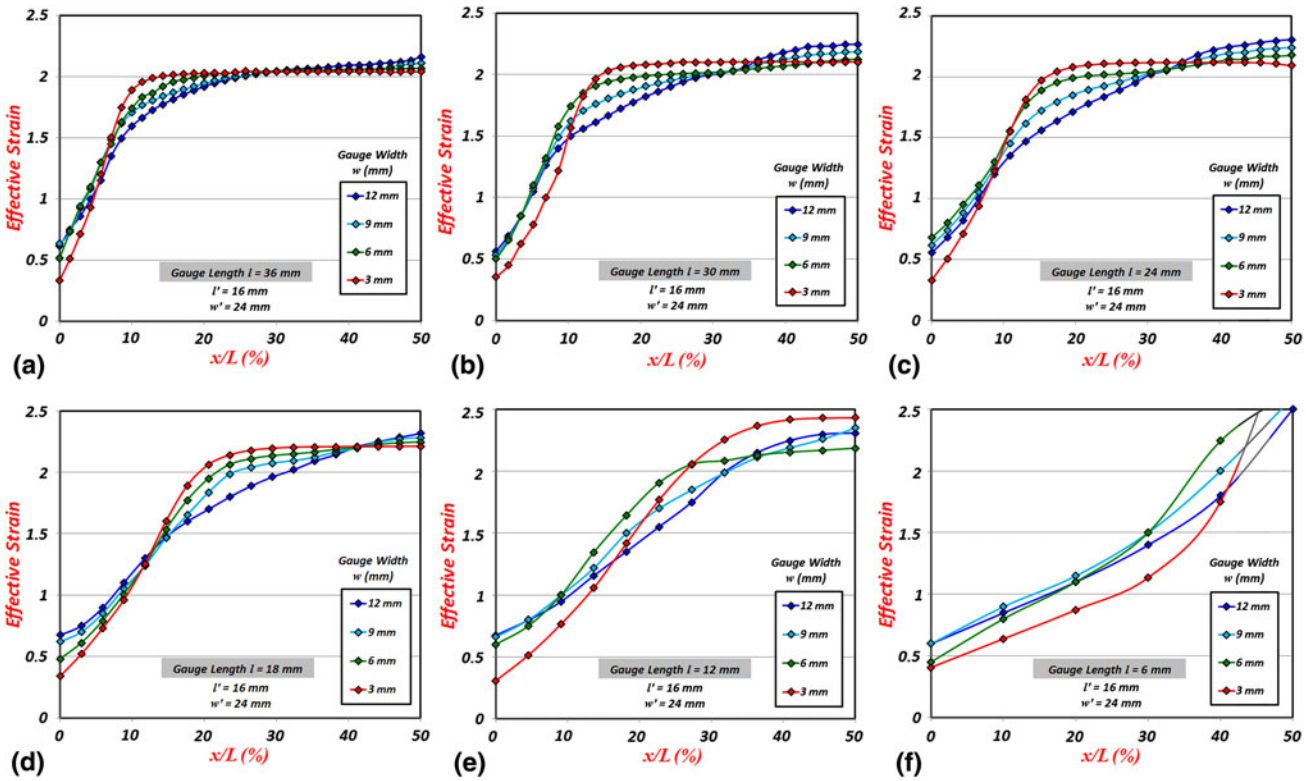

Fig. 10 Final strain distributions in specimens with various gauge widths and a gauge length of (a) 36 mm (b) 30 mm (c) 24 mm (d) 18 mm (e) 12 mm (f) 6 mm

same argument applies to the material flow data, where we generally observe that the results for the long specimen are unaffected by the approach, while the second approach yields lower errors for the short specimen.

It is now clear that following the approach of targeting "an overall theoretical strain" not only makes more practical sense, but also provides a better common basis for comparison, and delivers more prominent differentiation between the different geometries. Therefore, the simulations in the remainder of this study will be performed accordingly. The various sets of geometries in Table 2 will be considered individually, to understand the influences of the corresponding geometrical parameter(s), as we explore next.

4.2 Combined Effects of Gauge Length/Width

The first four sets of specimens in Table 2 are considered here, covering a total of 24 combinations of gauge length and width values. While maintaining the same grip region in all, the gauge length is varied between 6 and 36 mm in each set, and the gauge width is varied between 3 and 12 mm across the four sets. After stretching as previously described, and recording the developed strains; plots of strain distribution along the gauge region are shown in the four parts of Fig. 8. For the first set of specimens with 3 mm gauge width, Fig. 8(a) shows that the longer the specimen, the higher the deformation uniformity. The longest specimen shows uniform strains along roughly 80% of its gauge length. As the gauge length decreases, deformation uniformity is compromised, leading to higher levels of strain localization at the center of the specimen. This might not be critical initially, but it becomes unmistakably evident as we approach the shortest specimen. Most importantly, these results indicate that only a portion of the specimen can be claimed to experience the imposed strain rate; the remaining parts of the specimen are effectively undergoing lower or higher rates.

By moving to the second set of specimens with a 6 mm gauge width, Fig. 8(b) demonstrates an essentially similar trend, although with less uniform strains. A quick one-to-one comparison shows that the 36 mm specimen, for instance, does not experience the same deformation uniformity level of the 36 mm specimen in Fig. 8(a). This can be mainly linked to the AR-Gauge ratio, which ranges between 2 and 12 for the first set, compared with 1 to 6 for the second set. To confirm the aforementioned, one shall consider the remaining two sets, and the corresponding strain distribution curves in Fig. 8(c) and (d). Since the gauge width increases to 9 and 12 mm, respectively, the AR-Gauge values decline furthermore. The result is even lower deformation uniformity, as it is particularly the case with the curves in Fig. 8(d), with the lowest range of AR-Gauge values. In conclusion, these curves indicate that the higher the gauge length-to-width ratio, the more uniform the deformation is expected to be.

Additional examination of Fig. 8 indicates that another factor, beside the AR-Gauge ratio, is playing a role. Each of the four parts contains a curve corresponding to the same AR-Gauge ratio; nonetheless, those curves are not identical. A clear example is provided by considering the 6 mm specimen in Fig. 8(a) and the 24 mm specimen in Fig. 8(d). Both the specimens share an AR-Gauge ratio of 2; yet when compared, they are largely different, as evident from Fig. 9. Considering that the grip region is maintained the same for all the specimens, every increase in the gauge width results in a decrease in the AR-GG ratio. The previous two curves have AR-GG ratios of 8 and 2, respectively. This large variation has definite impact on the way the material flows into the gauge region, hence affecting deformation uniformity. Accordingly, the previous conclusion on the impact of the AR-Gauge ratio has to be coupled with the impact of AR-GG, to complete the picture.

A look back at the four parts of Fig. 8 indicates that for the specimens with large AR-Gauge ratios, dropping the AR-Grip ratio adversely affects deformation uniformity. To further support this, Fig. 10 shows the plots of strain distribution in the 24 specimens, clustered by their gauge length. With the gauge length being fixed in each plot, it is evident that decreasing the gauge width, hence increasing both the AR-Gauge and the AR-GG ratios, enhances uniformity. This is most obvious with the 36 mm long specimens in Fig. 10(a). Only in parts (e) and (f) of the figure that the trend is unclear, mainly because the gauge length is at its smallest values of 6 and 12 mm. It is, therefore, generalized that enhanced tensile deformation is achieved in specimens with larger AR-Gauge and AR-GG ratios.

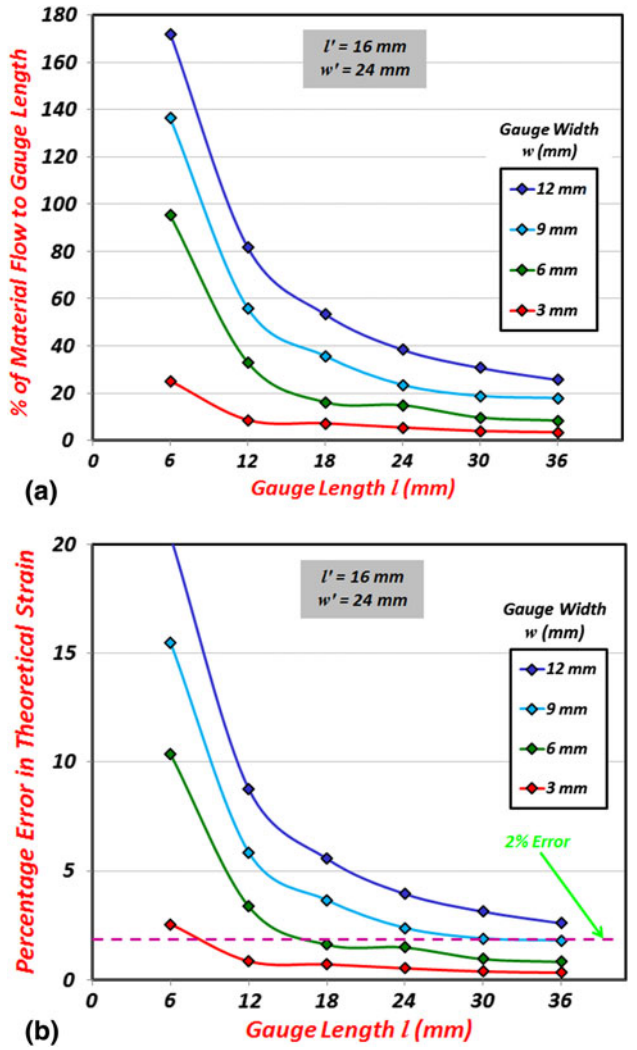

Fig. 11 (a) Percentage of material flow to gauge length (MF/*l*) for various combinations of gauge length and width values (b) the corresponding percentage error in the overall theoretical strain

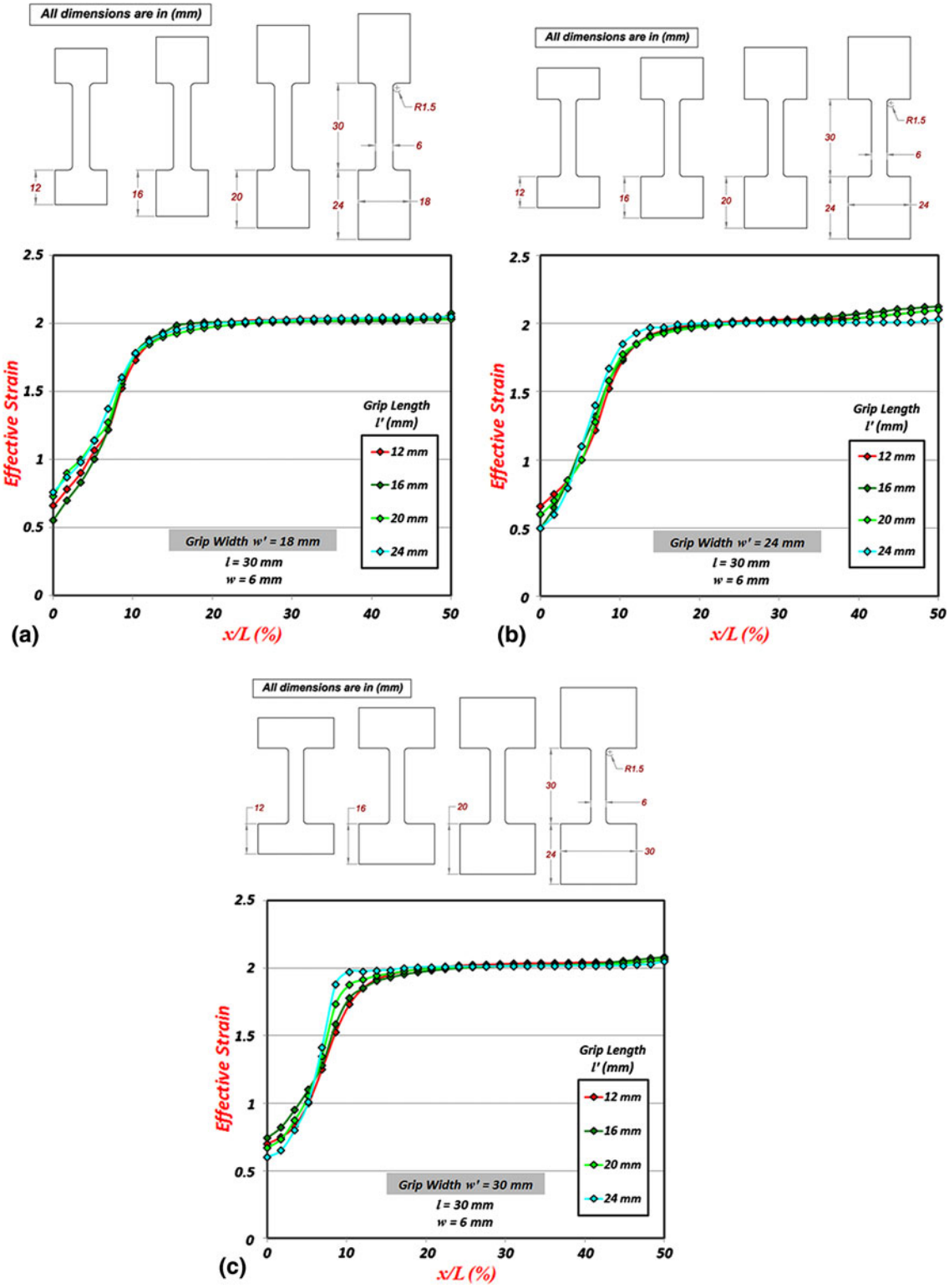

Fig. 12 Strain distribution in four identical specimens except for the grip length changing between 12 and 24 mm, where the grip width is (a) 18 mm (b) 24 mm (c) 30 mm

The focus was then directed toward material flow, which was evaluated for all the specimens after considering the partitioned deformed grip region in each. To make the comparison between the different specimen geometries viable, material flow was normalized with respect to the initial gauge length, and the results are plotted in Fig. 11(a). The four curves clearly show that decreasing the gauge length escalates the material flow problem, especially when the gauge length drops below 12 mm, where material flow exceeds 50% of the gauge length in most cases. Moreover, for any given gauge length, increasing the gauge width seems to adversely affect material flow. On the whole, when considering the corresponding

AR-Gauge and AR-GG ratios, these results agree well with the previous ones where the combined effects of gauge length and width on the overall strain distribution and deformation uniformity were studied.

Finally, to draw some guidelines on how to select the proper proportions of a specimen geometry, the curves in Fig. 11(a) were used to estimate the error in the overall theoretical strain associated with material flow in each specimen. The outcome is presented in Fig. 11(b), the curves of which follow similar trends to those in part (a). In this case, however, one can relate the initial geometry to a measurable important quantity, which is the overall theoretical strain. By targeting an arbitrary error level of 2%, for instance, Fig. 11(b) suggests that the gauge width should not be greater than 9 mm; preferably, it should be less than or equal to 6 mm. As for the gauge length, the minimum value is apparently dependent on the gauge width; yet all the curves point to a gauge length value that is at least three times the gauge width.

Conclusively, the results recommend that both the AR-Gauge and the AR-GG ratios should assume values larger than or equal to 3. Naturally, the investigator can target much higher ratios for better performance; however, equipment limitations should be taken into account before doing so. One must not forget the large strains, hence the displacements, associated with testing superplastic materials. Therefore, starting with a large gauge length (higher than 35 mm) would be impractical in most cases, since heating chambers are limited in their cavity size, and some tensile testing machines have very limited strokes. All things considered, we suggest an AR-Gauge ratio of 4 and an AR-GG ratio of 4, as the optimum values for a superplastic tensile test specimen. These guidelines not only assure minimal material flow, but also fine deformation uniformity, as evident when considering the plots in Fig. 8 and 10.

4.3 Combined Effects of Grip Length/Width

Naturally, the grip region is expected to play a secondary role to that of the gauge region; nonetheless, a portion of this comprehensive investigation is dedicated to studying and quantifying its effects. Twelve specimen geometries, embodying the last three sets in Table 2, are considered here. In all, a 30 mm gauge length and a 6 mm gauge width are maintained, while the grip region's proportions are changed. The grip length is varied between 12 and 24 mm in each set, and the grip width is varied between 18 and 30 mm across the three sets. All the specimens were stretched, as previously described, to an overall theoretical strain of 1.75, and the resulting strain distributions along the specimen's gauge were plotted in Fig. 12. Not surprisingly, the curves show little disparities, and one must look really close to notice the difference between them. For the specimens with the smallest grip width, Fig. 12(a) shows no apparent influence on deformation within the specimen; only insignificant variation is noticed near the grip area. As we move toward the specimens with the greatest grip width of 30 mm in Fig. 12(c), the curves deviate from each other, indicating somewhat higher deformation uniformity as the grip length increases. On the other hand, a general comparison between the three parts of Fig. 12 shows that a larger portion of the specimen exhibits uniform strains as the grip width increases.

The slight impact of the grip region on material deformation must be indirectly caused by small material flow. The gauge region's size (30×6 mm) was selected based on the results from Fig. 11(b), so that insignificant material flow is to take place (around 10% of the gauge length). By changing the proportions of the grip region, thereafter, one can establish and quantify its influences on material flow. A plot of the ratio of material flow to the initial gauge length (MF/l) for all the 12 specimens is shown in Fig. 13. Although material flow follows a decreasing trend as the size of the grip region increases, the effect is still small and the changes are minor. At least, this agrees with the equally slight improvement in deformation uniformity as the size of the grip region increases.

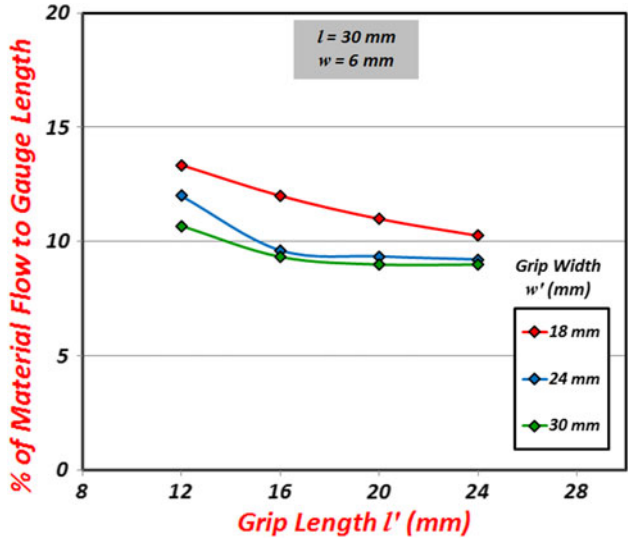

Fig. 13 Percentage of material flow to gauge length (MF/l) for various combinations of grip length and width values

On the whole, it is certainly clear that selecting the size of the grip region is secondary to that of the gauge region, yet a good selection of its proportions helps refine the performance of the test specimen. Since the gauge width is fixed in all the considered specimens, the results presented here can be generalized in terms of both the AR-Grip and the AR-GG ratios. The refined deformation uniformity in Fig. 12(b) and (c) suggests that the AR-GG ratio should be higher than 3; this agrees with the conclusion derived from the previous section. The AR-Grip ratio, on the other hand, is suggested to be greater than 0.5; note how the specimens in Fig. 12(a) show no disparities, since they all have an AR-Grip ratio higher than 0.5. Ultimately, physical limitations in the gripping device and the testing machine should be considered in determining the values of these ratios.

5. Summary

In a comprehensive FE-based investigation, the effects of specimen geometry on the outcome of a superplastic tensile test were examined, covering a wide range of gauge length, gauge width, grip length, and grip width values. The simulations were carried out on the Ti6Al4V titanium alloy at 900 °C, due to its excellent superplastic behavior. An artificial partition was applied between the grip and the gauge regions of each specimen before stretching, to ease monitoring two targeted outcomes; deformation uniformity along the gauge length, and

the amount of material flow from the grip into the gauge region. Two simulation approaches, targeting a maximum localized strain versus targeting an overall theoretical strain, were first analyzed and compared, to identify their influences on the results. By adopting the latter as the better approach, the investigation demonstrates how the variations in specimen geometry could lead to large disparities in testing results, hence stressing the need for adopting unified standard specimen geometry for the uniaxial tensile testing of superplastic materials. The results suggest that such a unified geometry should optimally have a gauge length to width ratio of 4, as well as a grip to gauge width ratio of 4. As for the grip region's proportions, they are not as critical as the gauge region, and a grip width to length ratio of 1.5 should suffice.

References

1. "Method for Evaluation of Tensile Properties of Metallic Superplastic Materials," JIS H 7501, 2002
2. "Standard Test Method for Determining the Superplastic Properties of Metallic Sheet Materials," ASTM E2448, 2005
3. "Method for Evaluation of Tensile Properties of Metallic Superplastic Materials," BS ISO 20032, 2007
4. H. Watanabe, A. Takara, H. Somekawa, T. Mukai, and K. Higashi, Effect of Texture on Tensile Properties at Elevated Temperatures in an AZ31 Magnesium Alloy, *Scripta Mater.*, 2005, **52**, p 449–454
5. P. Mukhopadhyay, S. Biswas, and A. Chokchi, Deformation Characterization of Superplastic AA7475 Alloy, *Trans. Indian Inst. Met.*, 2009, **62**(2), p 149–152
6. J. Liu, D. Chen, Z. Chen, and H. Yan, Deformation Behavior of AZ31 Magnesium Alloy During Tension at Moderate Temperatures, *J. Mater. Eng. Perform.*, 2009, **18**(7), p 966–972
7. F. Abu-Farha and M. Khraisheh, Analysis of Superplastic Deformation of AZ31 Magnesium Alloy, *J. Adv. Eng. Mater.*, 2007, **9**(9), p 777–783
8. J. Chang, E. Taleff, and P. Krajewsky, Effect of Microstructure on Cavitation during Hot Deformation of a Fine-Grained Aluminum-Magnesium Alloy as Revealed through Three-Dimensional Characterization, *Metall. Mater. Trans. A*, 2009, **40**(13), p 3128–3137
9. K. Johnson, M. Khaleel, C. Lavender, S. Pitman, J. Smith, M. Smith, and C. Hamilton, The Effect of Specimen Geometry on the Accuracy of Constitutive Relations in a Superplastic 5083 Aluminum Alloy, *Mater. Sci. Forum*, 1994, **170–172**, p 627–632
10. F. Abu-Farha and R. Curtis, Quick-Mount Grips: Towards an Improved Standard for Uniaxial Tensile Testing of Metallic Superplastic Sheets, *Mat.-wiss. u. Werkstofftech.*, 2009, **40**(11), p 836–841
11. P. Bate, N. Ridley, and K. Sotoudeh, Effect of Gauge Length in Superplastic Tensile Tests, *Mater. Sci. Technol.*, 2008, **24**(10), p 1265–1270
12. X. Ding, H. Zbib, C. Hamilton, and A. Bayoumi, On the Optimization of Superplastic Blow-Forming Processes, *J. Mater. Eng. Perform.*, 1995, **4**(4), p 474–485